 DOI:10.30420/566414035

Analysis of Coupling Mechanism and Decoupling between Inductor and Active Filter in Hybrid EMI Filter

Han BU, Fanghua ZHANG, Chuang ZHOU

Department of Electrical Engineering, Nanjing University of Aeronautics and Astronautics, China

Corresponding author: Han Bu, e-mail-address:buh123@nuaa.edu.cn
Speaker: Han Bu, e-mail-address:buh123@nuaa.edu.cn

Abstract

As wide-band semiconductors mature, their higher switching frequency generates serious EMI. Hybrid EMI filters can effectively suppress EMI while reducing the size of the filter. In this paper, the effect of coupling between the active part and the common mode inductor in the hybrid EMI filter is investigated, and a cancellation part decoupling circuit is designed for the performance problems caused by its coupling to ensure the stability of the filter; after that, in order not to affect the performance of the active part, the decoupling design is carried out in the sense part on the basis of the previous design, so that the filter can work stably in the test frequency band without affecting its performance at the same time. Subsequently, the effect of the filter in a square wave noise source and an isolated DC/DC converter is tested, and the experimental results show that the HEF designed in this paper has a good noise suppression effect.

1 Introduction

With the development and maturity of wide-bandwidth devices such as SiC, GaN, the converter switching frequency is greatly increased, and serious Electromagnetic Interference (EMI) noise is generated due to its higher du/dt and di/dt during conduction and turn-off. Higher EMI may lead to operational failures of circuits, as well as system EMI exceedances. In order to make the power electronic equipment under test meet the appropriate Electromagnetic Compatibility (EMC) standards, it is usually necessary to add EMI filters to the main circuit to suppress the EMI of the system [1]. As one of the main measures to solve the EMI problem, filters need to be placed at the inputs and outputs of electronic devices that are severe or very sensitive to external interference, so that the EMI is attenuated and the EMC performance of the system can be improved .There are two main types of EMI filters: passive EMI filters (PEF) and Active EMI filters (AEF). PEF mainly uses inductors and capacitors to attenuate EMI, while AEF mainly uses transistors and operational amplifiers to inject compensating voltages or currents into circuits to attenuate EMI.

PEF has been maturely applied and commercialized for a long time [2]. Since power electronic systems are gradually developing towards high power density, the EMI filter design method for system power density is a hot research topic at present, and AEF is a very effective method to improve the system power density. [3] designed an AEF capable of suppressing both Common-Mode (CM) and Differential-Mode (DM) noise without significant increase in size, respectively. [4-5] carried out the design of DM active filter based on modeling of DM AEF and stability analysis respectively. The active filter is analyzed based on the developed DM noise model.

AEF can effectively suppress low-frequency EMI, while PEF can effectively suppress high-frequency EMI. In order to further improve the power density of the system and to combine the advantages of the two types of EMI filters, the design of Hybrid EMI filter (HEF) has become a hot research topic. [6] designed active EMI filters based on LCL-type filters and integrated with improved LCL-LC filters as hybrid filters to suppress EMI noise. [7] analyzed the CM noise propagation path based on the motor drive system and proposed to embed the analog AEF at the common mode grounding point to suppress the CM noise, which greatly reduces the size of the CM filtering component. [8] modeled and analyzed each component of a co-modeled HEF separately, and then superimposed each part of the model to obtain an overall model of the HEF with good model accuracy. [9] presents a common mode choke with integrated common mode detection and suppression for HEFs, which effectively reduces the size of the filter.

In the above literature study, due to the volume limitation of the PEF and the high frequency loop gain limitation of the analog AEF, the integration of passive and active EMI filters is a feasible solution for EMI suppression, but there is little literature for the instability generated by the coupling between the PEF and the AEF, this

ISBN 978-3-8007-6414-3

paper analyzes the possible instability of the HEF and proposes a solution to increase the stability of the system. This paper analyzes the possible instability of HEF and proposes a solution to increase the stability of the system.

2 HEF Modeling Analysis

In the next sections, this paper will model and analyze the stability of each component in the hybrid EMI filter, derive the filter gain and analyze the causes of instability.

Analog AEF can be classified as either voltage or current based on the way the noise signal is sampled as well as cancellation, with voltage elimination requiring a voltage cancellation. Similar to the current transformer Transformer, the voltage injector is bulky due to the nature of the input current and may not result in an overall size reduction. Therefore, in this paper, a Voltage Sense Current Cancellation (VSCC) topology is used, which employs a high safety rated voltage capacitor without the need for a transformer. Also a feedback type connection is chosen for more system stability. The schematic of the final filter is shown in Fig. 1.

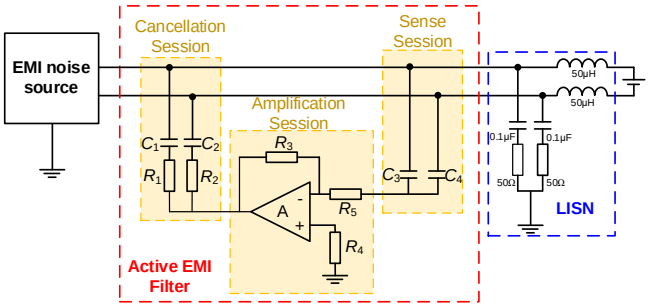

Fig. 1. Active EMI filter under investigation

2.1 Feedback VSCC type AEF principle

As shown in Fig. 1, Feedback VSCC type AEF is mainly composed of sensing, amplification, Cancellation of three parts, inverted amplification through the sampling of noise signals injected back into the circuit for noise cancellation, thereby reducing the noise current, and reduce the amplitude of EMI. According to the characteristics of the loop gain, the overall gain of the filter is the product of the three partial gains.

$$G = G_1 G_2 G_3 \tag{1}$$

The sense circuit is essentially a high-pass filter that samples harmonics in the desired test frequency range. It consists of an RC series circuit where capacitor C_3, C_4 is rated for the input voltage and additional safety ratings are required. The transfer function of the sampling circuit is given by the following equation. where resistor R_5 is shared by the amplification and sense session. The transfer function of the sense circuit is given by the following (2).

$$G_1 = \frac{sC_3R_5}{sC_3R_5 + 1} \tag{2}$$

As shown in Fig. 1, the amplification session is an inverting amplifier, which is essentially a negative feedback system consisting of an operational amplifier and its external feedback circuit. The amplifier has been modeled in detail in [8], but the model is complex and most of the parameters need to be obtained from datasheets, which can lead to inaccuracies in the parameters due to differences in the devices, thus distorting the model. The operational amplifier is the core device of the amplification chain, and the main factor determining the performance of the operational amplifier is its open-loop gain. As shown in Fig. 2 show the amplitude-frequency curve of the open-loop gain of the operational amplifier, the open-loop gain of the operational amplifier is a constant G_0 only in the frequency range from DC to f_0, and after f_0, the gain decreases with a slope of approximately 20dB/dec, and has been decreasing to 0dB at f_t, where the frequency f_t is the frequency of the operational amplifier's unit gain.

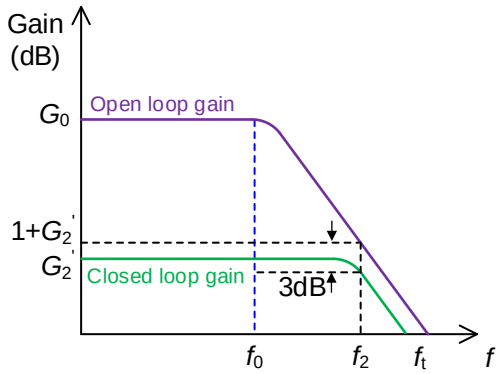

Fig. 2. Amplitude-frequency curve of op-amp gain

The closed-loop gain G_2 provided by the amplification link is simultaneously determined by the open-loop gain of the operational amplifier and the external feedback circuit. When the feedback circuit gain G_2' is much smaller than the open-loop gain of the operational amplifier, the closed-loop gain G_2 is equal to the feedback gain G_2'; when the open-loop gain curve is close to G_2', the closed-loop gain curve G_2 begins to decline with the same 20dB/dec speed as that of the open-loop gain curve, and the gain of turning frequency f_2 is G_2'. From the frequency point where G_2' drops by 3dB, the open loop gain corresponding to the f_2 frequency point is $1+G_2$', which can be obtained to the amplification gain G_2 as follows in (3)

$$G_2 = \frac{2\pi f_t}{(1+G_2')s + 2\pi f_t} \frac{R_3}{R_5} \tag{3}$$

Like the sense circuit, the cancellation circuit is also a high pass filter and the circuits for the L line as well as

 DOI:10.30420/566414035

the N line are composed of by R_1, $C_1$and R_2, C_2 respectively. The transfer function of the injection network is given by the following equation: (4):

$$G_3 = \frac{sC_1}{sC_1R_1 + 1} \tag{4}$$

2.2 HEF stability analysis

The substantial filtering effect of the VSCC feedback topology is equivalent to a passive device with an impedance of 1/G connected in parallel between the noise source and the load[10], which serves to provide a low-impedance path for the noise signal so that the noise signal does not flow through the load, thus realizing the filtering effect.The VSCC feedback active filtering topology is equivalent to a low-impedance passive device connected in parallel in the loop, and the DC/DC-type converter is a high source impedance, and the common mode impedance of the LISN is generally considered to be low impedance, at this time between the AEF and the LISN to add a high impedance device can be consistent with the principle of impedance mismatch, that is, to add a common-mode inductance can be realized. The structure of the HEF selected in this paper is shown in Fig. 3.

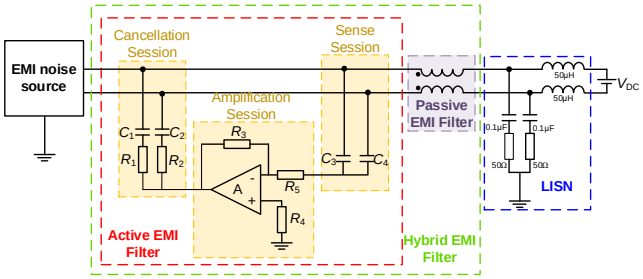

Fig. 3. Hybrid EMI filter under investigation

The filter insertion realizes the impedance mismatch between the input measurement and the output measurement, which proves the correctness of the active filter topology selection rules. At this point the system signal flow diagram is shown in Fig. 4.

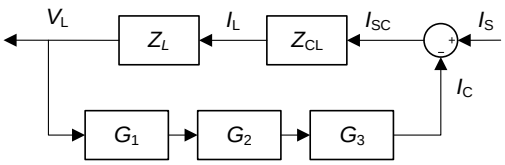

Fig. 4. Signal flow diagram

where Z_{CL} is the impedance of the CM choke, I_S is the noise current, and V_L and I_L are the voltage and current detected by the LISN respectively.

According to the transfer function derived from the signal flow diagram can be drawn the response of the system bode diagram as shown in Fig. 5, From Fig. 5, it can be seen that there are low-frequency poles in the system, the phase is greater than 180 ° when the gain is over 0, and the gain shows a trend of growth, and its indication of negative gain margin. This phenomenon can make the system unstable. At this time the op amp feedback state is uncertain, not only will not compensate for EMI noise, but even inject noise.

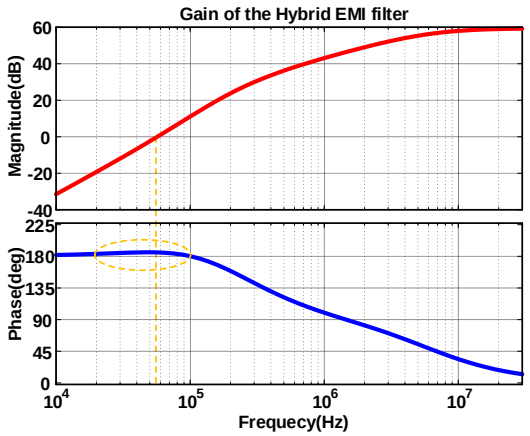

Fig. 5. Loop gain of HEF

3 Design and analysis of decoupling circuits

According to the analysis in the previous section, the hybrid EMI filter is unstable in the low-frequency band, and by analyzing the filter structure, this phenomenon is mainly due to the LC resonance between the CM choke and the cancellation capacitance, and the scattering parameter in the electromagnetic field theory is utilized to characterize the external properties of the EMI filter, S-parameters can be measured using a vector network analyzer(VNA) and the measured results are obtained as shown in Fig. 6, which shows that the HEF in low-frequency band there has a resonance point, which makes the performance of the filter degraded greatly. Under this circumstance, in order to achieve sufficient EMI noise attenuation, a larger CM choke should be required, which greatly increases the size of the filter.

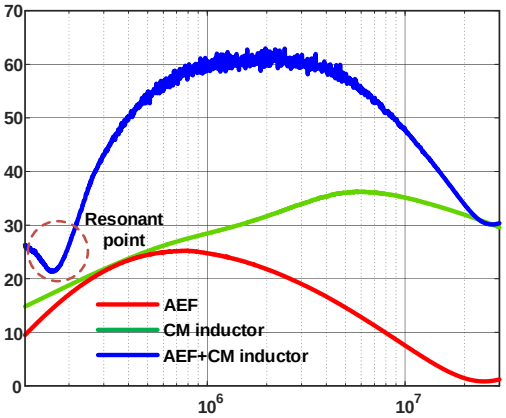

Fig. 6. Insertion loss obtained by using a VNA

3.1 Cancellation session decoupling design

In order to solve the stability problem of the filter, a decoupling circuit in the cancellation circuit is proposed in this paper. Firstly, in order to suppress the resonance, a resistor is added as a damping in the cancellation circuit, which serves to eliminate the low-frequency poles. Although the resistor can suppress the resonance, it also deteriorates its performance. In order to minimize its effect on the high-frequency performance, an RC parallel circuit is used as the decoupling circuit, with the resistor R_S as the damping to suppress the resonance, and the capacitor C_S to compensate for the high-frequency performance. The transfer function of the cancellation session after adding the decoupling circuit show in (5).

$$G_{3D} = \frac{s^2(C_1C_sR_s)+sC_1}{s^2(C_1R_5R_sC_s)+s(C_1R_5+C_sR_s+C_1R_s)+1} \quad (5)$$

Cancellation capacitor is directly connected to the high-voltage bus side, it needs a large volume of high-voltage capacitance, and the circuit and amplifier part connected in the middle of the capacitor will only flow through the noise signal, so it can be selected as an SMD device, which will not have an impact on the volume and weight of the filter. The circuit diagram after adding the decoupling circuit is shown in Fig. 7.

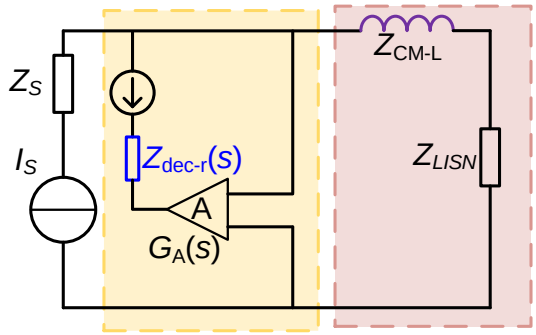

Fig. 7. HEF including cancellation session decoupling

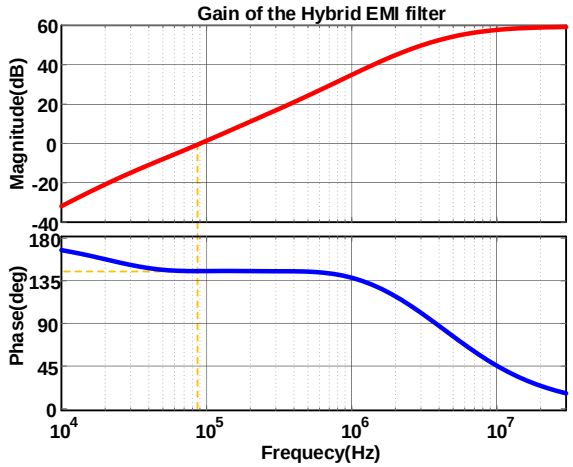

Fig. 8. Loop gain after cancellation circuit compensation

where Zdec-r is the impedance of the decoupling circuit. The response of the system bode graph as shown in Fig. 8, it can see the system in the gain over 0 when the phase is less than 180 °, about 30° degrees of phase margin, the system is more stable operation, but at this time the value of the decoupling resistor reaches 1.2k, which will lead to the AEF compensation current ability to become weaker.

3.2 Sense session decoupling design

In order to maintain the Sense waveform without distortion while not affecting the bandwidth of the sampling circuit, a capacitor connected in parallel to the resistor is a good choice, and by reasonably adjusting the values of resistor and capacitor it is possible to minimize the resulting phase shift in the vicinity of the gain-over-zero point. The adjusted bode plot is shown in Fig. 9. The resonance point between the CM choke inductor and the capacitor is changed, the phase margin reaches 45° degrees, while the value of the decoupling resistor measured by the compensation is reduced to 47Ω, which almost does not affect the cancellation current.

$$G_{1D} = \frac{sC_3R_5}{sC_3R_5+sC_rR_5+1} \quad (6)$$

Two decoupling circuits are added to the AEF designed in this paper: the RC parallel circuit in the Cancellation circuit and the bypass capacitor in the Sense circuit, respectively, at which time the topology of the AEF circuit is shown in Fig. 10.

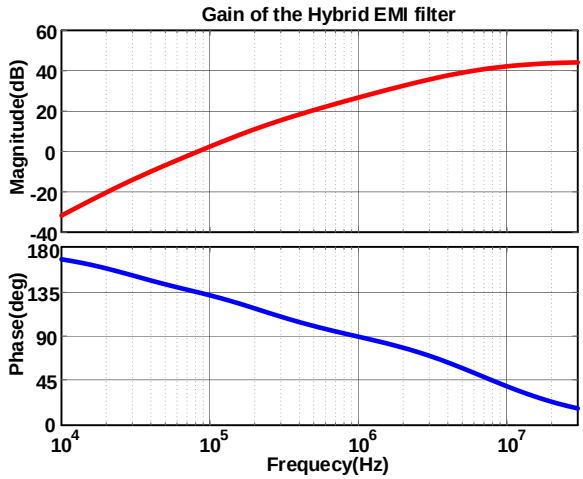

Fig. 9. Loop gain after double compensation

The insertion loss was measured using VNA, as shown in the Fig. 11, the resonance point has been eliminated and the insertion loss at the low frequency is boosted by up to 11dB.

 DOI:10.30420/566414035

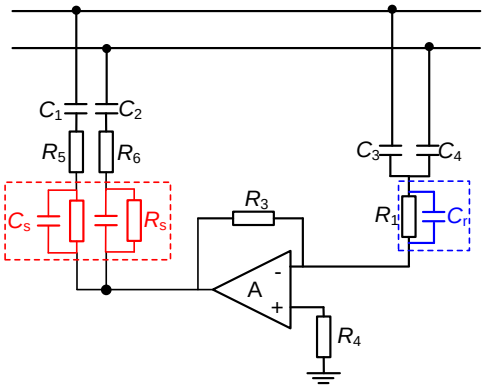

Fig. 10. AEF with decoupling circuit

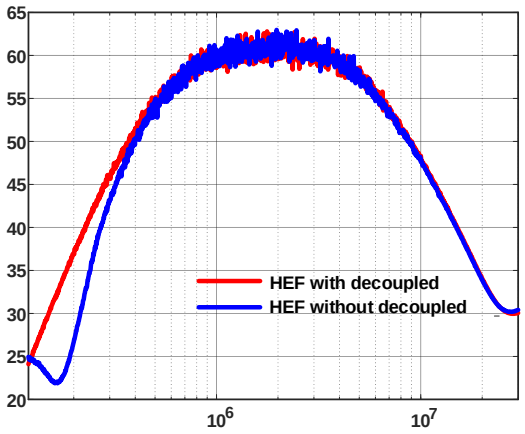

Fig. 11. IL obtained by using a VNA

4 Experimental results

To further validate the stability analysis, a signal generator with 50Ω source impedance was used as a noise source. A 500mV 150kHz square wave was fed into the HEF. The measurement results are shown in Fig. 12.

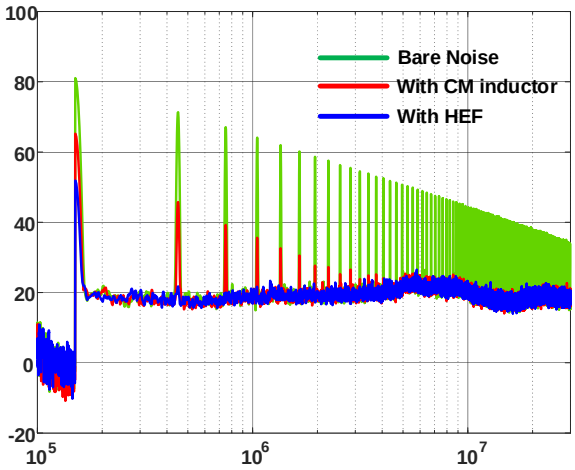

Fig. 12. CM noise measured with a 150kHz square wave from signal generator

It can be seen that the HEF can provide effective EMI attenuation at the previously unstable frequency band with no instability.

Tab. 1. Key parameters of HEF

Parameter	Value
Sense capacitor, C_3, C_4	2.2nF
Cancellation capacitor, C_1, C_2	22nF
Sense resistor, R_5	2.2kΩ
Cancellation resistor, R_1, R_2	220Ω
Feedback resistor, R_3	220kΩ
Cancellation decoupling, C_S, R_S	2.2nF,47Ω
Sense decoupling, C_r	10nF

In order to verify the performance of the CM HEF of this design, a 270/28V rated 3kW LLC-DCX+Buck two-stage DC/DC converter prototype is used as a test object, with the two stages operating at a switching frequency of 400kHz and 200kHz, respectively. The main system parameters of the test equipment and the HEF are shown in Tab 1. The LISN and noise separator networks are connected between the power supply and the HEF. The EMI receiver is an CYBERTEK EM5080B with a setup range of 150 kHz to 30 MHz as specified in the CISPR 22 EMI standard.

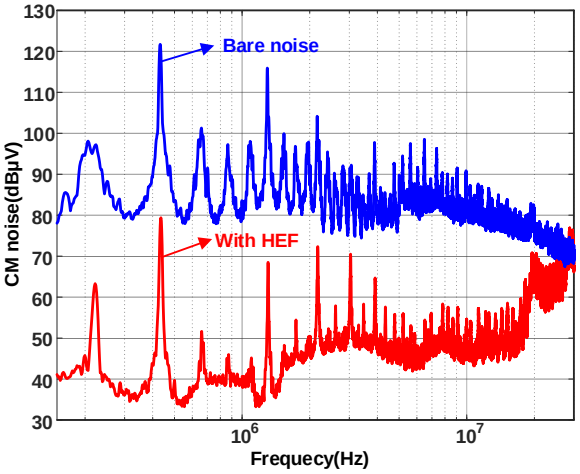

Fig. 13. Conducted CM noise spectrum

The blue line in Fig. 13 shows the original common-mode noise spectrum of the DC/DC converter operating without any filter, and the red line in Fig. 13 shows the noise spectrum of the DC/DC converter with the HEF designed in this paper connected in the circuit. It can be seen that the filter designed in this paper provides good noise attenuation in the frequency band before 10MHz, providing about 50dB attenuation amplitude at the highest point, but the attenuation effect is poor after 10MHz, and even increases the noise after 20MHz, which is mainly due to two reasons: 1) the inductor and capacitor used in this design have poor high-frequency performance, and the self-resonance frequency is in the noise test band, which makes the inductor and capacitor lose their filtering and compensating ability in the high-frequency band; 2) due to the limitation of the operational

amplifier performance bandwidth, the high-frequency band has already exceeded the operational amplifier's operating range, which makes the output distortion bring additional noise. These issues will be studied later.

Overall the HEF designed in this paper is able to suppress EMI noise and does not suffer from instability.

5 Conclusion

In this paper, a decoupling method for hybrid EMI filters is designed. The mathematical model of HEF is firstly established. The stability of the AEF and HEF is further analyzed and a decoupling circuit is designed for the problem of low frequency poles in the HEF, which improves the instability of the HEF and increases the Noise Suppression Capability in the low-frequency band. The experimental results show the effectiveness of the proposed method. The method proposed in this paper can also be applied to other types of HEFs.

6 References

[1] S. Ogasawara and H. Akagi, "Modeling and damping of high-frequency leakage currents in PWM inverter-fed AC motor drive systems," in IEEE Transactions on Industry Applications, vol. 32, no. 5, pp. 1105-1114, Sept.-Oct. 1996.

[2] Y. Maillet, R. Lai, S. Wang, F. Wang, R. Burgos and D. Boroyevich, "High-Density EMI Filter Design for DC-Fed Motor Drives," in IEEE Transactions on Power Electronics, vol. 25, no. 5, pp. 1163-1172, May 2010.

[3] Y. Zhou, W. Chen, X. Yang, R. Zhang, R. Yan, et al., "A New Integrated Active EMI Filter Topology With Both CM Noise and DM Noise Attenuation," in IEEE Transactions on Power Electronics, vol. 37, no. 5, pp. 5466-5478, May 2022.

[4] B. Narayanasamy, F. Luo and Y. Chu, "Modeling and Stability Analysis of Voltage Sensing based Differential Mode Active EMI Filters for AC-DC Power Converters," 2018 IEEE Symposium on Electromagnetic Compatibility, Signal Integrity and Power Integrity (EMC, SI & PI), Long Beach, CA, USA, 2018, pp. 322-328.

[5] R. Goswami, S. Wang, E. Solodovnik and K. J. Karimi, "Differential Mode Active EMI Filter Design for a Boost Power Factor Correction AC/DC Converter," in IEEE Journal of Emerging and Selected Topics in Power Electronics, vol. 7, no. 1, pp. 576-590, March 2019.

[6] J S. Jiang, Y. Liu, W. Liang, J. Peng and H. Jiang, "Active EMI Filter Design With a Modified LCL-LC Filter for Single-Phase Grid-Connected Inverter in Vehicle-to-Grid Application," in IEEE Transactions on Vehicular Technology, vol. 68, no. 11, pp. 10639-10650, Nov. 2019.

[7] Y. Zhang and D. Jiang, "An Active EMI Filter in Grounding Circuit for DC Side CM EMI Suppression in Motor Drive System," in IEEE Transactions on Power Electronics, vol. 37, no. 3, pp. 2983-2992, March 2022.

[8] Y. Chu, S. Wang and Q. Wang, "Modeling and Stability Analysis of Active/Hybrid Common-Mode EMI Filters for DC/DC Power Converters," in IEEE Transactions on Power Electronics, vol. 31, no. 9, pp. 6254-6263, Sept. 2016.

[9] L. Dai, W. Chen, X. Yang, M. Zheng, Y. Yang and R. Wang, "A Multi-Function Common Mode Choke Based on Active CM EMI Filters for AC/DC Power Converters," in IEEE Access, vol. 7, pp. 43534-43546, 2019.

[10] Z. Zhang and A. M. Bazzi, "A Virtual Impedance Enhancement Based Transformer-Less Active EMI Filter for Conducted EMI Suppression in Power Converters," in IEEE Transactions on Power Electronics, vol. 37, no. 10, pp. 11962-11973, Oct. 2022.

